Relationships between radiosonde and RUC-2 meteorological conditions and cloud occurrence determined from ARM data

Patrick Minnis, Yuhong Yi, Jianping Huang, and Kirk Ayers
NASA Langley Research Center, Hampton, Virginia, USA

Received 21 March 2005; revised 18 June 2005; accepted 7 September 2005; published 3 December 2005.

[1] Relationships between modeled and measured meteorological state parameters and cloudy and cloud-free conditions are examined using data taken over the ARM (Atmospheric Radiation Measurement) Southern Great Plains Central Facility between 1 March 2000 and 28 February 2001. Cloud vertical layering was determined from the Active Remotely Sensed Cloud Location product based on the ARM active sensor measurements. Both temperature and relative humidity (RH) observations from balloon-borne Vaisala RS80-15LH radiosonde (SONDE) and the Rapid Update Cycle (RUC) 40-km resolution model are highly correlated, but the SONDE RHs generally exceed those from RUC. Inside cloudy layers, the RH from SONDE is 2–14% higher than the RH from RUC at all pressure levels. Although the layer mean RH within clouds is much greater than the layer mean RH outside clouds or in clear skies, RH thresholds chosen as a function of temperature can more accurately diagnose cloud occurrence for either data set than a fixed RH threshold. For overcast clouds (cloud amount greater than or equal to 90%), it was found that the 50% probability RH threshold for diagnosing a cloud, within a given upper tropospheric layer, is roughly 90% for the SONDE and 80% for RUC data. For partial cloud cover (cloud amount is less than 90%), the SONDE RH thresholds are close to those for RUC at a given probability in upper tropospheric layers. Cloud probability was found to be only minimally dependent on vertical velocity. In the upper troposphere, SONDE ice-supersaturated air occurred in 8 and 35% of the clear and cloudy layers, respectively. The RH was distributed exponentially in the ice supersaturated layers as found in previous studies. The occurrence of high-altitude, ice-supersaturated layers in the RUC data was roughly half of that in the SONDE data. Optimal thresholds were derived as functions of temperature to define the best RH thresholds for accurately determining the mean cloud cover. For warm clouds the typical SONDE threshold exceeds 87%, while the RH thresholds for cold clouds are typically less than 80% and greater than 90% with respect to liquid and ice water, respectively. Preliminary comparisons with satellite data suggest that the relationships between cloudiness and RH and T determined here could be useful for improving the characterization of cloud vertical structure from satellite data by providing information about low-level clouds that were obscured by high-level clouds viewed by the satellite. The results have potential for improving computations of atmospheric heating rate profiles and estimates of aircraft icing conditions. Similar analyses are recommended for later versions of the RUC analyses and forecasts.

Citation: Minnis, P., Y. Yi, J. Huang, and K. Ayers (2005), Relationships between radiosonde and RUC-2 meteorological conditions and cloud occurrence determined from ARM data, *J. Geophys. Res.*, *110*, D23204, doi:10.1029/2005JD006005.

1. Introduction

[2] Accurate characterization of the vertical and horizontal distribution of clouds and their properties is becoming increasingly important for a variety of weather and climate problems. One goal of the Atmospheric Radiation Measurement (ARM) Program [*Ackerman and Stokes*, 2003] is to improve the treatment of clouds and radiation in general circulation models (GCMs), ultimately to provide more reliable forecasts of climate. To achieve that goal, ARM has deployed continuously operating surface instruments in areas representing different climate regimes including a heavily instrumented central site and sparsely instrumented extended facilities to acquire more information about the spatial variability of the cloud and radiation fields. At the ARM Southern Great Plains (SGP) Central Facility (SCF), a variety of passive and active sensors provide detailed information about the vertical structure [e.g., *Clothiaux et al.*, 2000] and microphysical properties of clouds [e.g.,

0148-0227/05/2005JD006005$09.00

Mace et al., 1998a] passing over the site, but cannot provide depictions of the large- and meso-scale variability of the cloud structures that must be accurately reproduced in weather and climate models. To address that need, ARM sponsors the analysis of satellite data to provide spatially continuous estimates of cloud properties and top-of-atmosphere radiative fluxes. Those data sets [e.g., *Minnis et al.*, 1995a, 2002] are used for a variety of problems including use for validation and for establishing boundary conditions for single-column model case studies [e.g., *Ghan et al.*, 2000]. The information content from the satellite data, however, is much diminished compared to the SCF data stream because only passive sensors are used. Most satellite retrieval techniques provide a reasonable assessment of cloud properties for single-layered clouds, but incur large errors whenever overlapping multilayered cloud systems are present.

[3] Assessment of the potential for aircraft icing conditions from satellite data is also compromised in pixels with overlapped multilayered clouds [*Minnis et al.*, 2004a]. Icing conditions tend to occur in relatively thick supercooled liquid clouds. When thin ice clouds occur above low-level clouds, the retrieved cloud temperature may be too low resulting in misclassification of a warm cloud as being supercooled. When a thick ice cloud overlies a low cloud, the satellite retrieval can only interpret the scene as an ice cloud. Thus, the presence or absence of a low-level supercooled water cloud underneath those clouds is often indeterminate from the satellite analysis yielding large areas with no information about icing potential. Finding a reliable means for diagnosing clouds underneath high clouds and determining the location of thin cirrus clouds over low clouds would be a significant step toward constructing three-dimensional (3-D) cloud data sets that could be used to address weather problems like icing or to assist climate studies like those engaged by the ARM program.

[4] A variety of multispectral techniques have been developed to address the problem of identifying and analyzing overlapped clouds observed from satellites. Most of those methods [e.g., *Baum et al.*, 1994; *Kawamoto et al.*, 2002; *Pavlonis and Heidinger*, 2004] require that the upper-level cloud optical depth (OD) is less than about 5 because the infrared radiances from the low cloud that could influence the satellite-observed radiances are nearly completely attenuated by the upper-level cloud. Thus, even with the correct imager spectral channels and perfect detection, it is still not possible to determine whether or not a low cloud exists beneath an ice cloud with OD > 5. Combined visible, infrared, and microwave techniques [*Lin et al.*, 1998; *Huang et al.*, 2005] are not limited by the ice cloud OD, except when precipitation occurs, but they can only be used over ocean when the requisite channels are available. Geostationary satellites, which can provide high temporal resolution coverage, do not carry microwave imagers. Thus, a supplemental approach is needed to help cover those cases when $OD_{ice} > 5$.

[5] Vertical profiles of temperature T and humidity from radiosondes can provide information about overlapping cloudiness at the locations where the sondes are launched. For example, *Poore et al.* [1995] used a relative humidity (RH) thresholding technique to define cloud layers from radiosonde profiles of T and RH. The results provide a climatological assessment of cloud layer thickness and base heights at 63 locations. *Chernykh and Eskridge* [1996] used a combination of temperature-dependent dew point depression thresholds and the signs of the second derivative of T and RH with height to specify fractional cloud cover in a layer. *Wang and Rossow* [1995] and *Wang et al.* [2000] took a similar approach but greatly increased the global and temporal coverage using up to 1200 stations. They used a relative humidity threshold of 83% as a layer boundary, but required at least one reading to exceed 87% to accept the layer as a valid cloud. Cloud layers were determined from historical radiosonde data that, over the United States of America, were limited to layers with $T > -40°C$ because of problems with the humidity measurements at lower temperatures. Differences in radiosondes used over the globe may also induce some biases especially for high clouds because of differences in the humidity sensors (see *Minnis et al.* [2004b] for discussion). *Naud et al.* [2003] compared the methods of *Chernykh and Eskridge* [1996] and *Wang and Rossow* [1995] with surface-based active sensors and concluded that the two radiosonde methods were generally consistent with each other and had detection efficiencies between 81 and 99% depending on the version of the given method and the complement of active sensors used. They also found that the *Wang and Rossow* [1995] thresholds tended to classify moist cloudless layers as cloudy but suggest that lower thresholds are needed at high altitudes. Overall, the results from these earlier studies have clearly demonstrated the value of radiosonde data for determining cloud vertical structure.

[6] Unfortunately, radiosondes are launched on a regular basis only twice per day from a relatively sparse network. Thus, their utility for defining cloud vertical variability is limited only to few locations at 0000 and 1200 UTC. Numerical weather analyses (NWA) such as the European Centre for Medium Range Forecasting (ECMWF) and the Rapid Update Cycle (RUC [see *Benjamin et al.*, 2004a]) analyses represent a potentially more useful RH-profile data set for determining cloud layering on a more continuous basis. However, it remains to be shown that such analyses can yield cloud detection probabilities that are similar to those taken directly from radiosonde measurements. Differences between actual soundings and those produced by NWAs may be significant, especially for cold cirrus clouds, which have not been related to radiosonde humidities at $T < -40°C$. Use of the vertical profiles from NWA analyses for cloud diagnosis in the manner of *Wang et al.* [2000] would require determination of the relationships between the modeled meteorological state parameters and the cloud properties in a given volume of air. To date, such relationships have not been developed in a systematic manner. *Mace et al.* [1997] categorized from 95-GHz radar reflectivities from cirrus clouds over Pennsylvania as a function of RUC-determined temperature and large-scale vertical motion. They found that cirrus occurrence appears to be related in a complex manner to large-scale meteorological factors, but they provided no information about RH dependence of the observed clouds. *Mace et al.* [1998b] used ARM millimeter-wave radar (MMCR) data to validate condensate output from the operational ECMWF forecast model but did not relate cloud occurrence to the RH profiles. *Naud et al.* [2003] analyzed 4 years of ARM

MMCR, lidar, ceilometer, and radiosonde data to validate radiosonde-based estimates of cloud locations but did not attempt to develop any new relationships. *Zhang* [2003] showed that cloud properties derived from a month of satellite over the ARM SGP have some distinct relationships with RUC-based meteorological conditions under which the clouds exist, and such relationships vary with cloud scale. Most of the clouds studied were convective in origin and their upper and lower boundaries were relatively uncertain because they were based on retrievals from passive satellite-observed radiances.

[7] With the availability of high temporal resolution Active Remotely Sensed Cloud Location (ARSCL [*Clothiaux et al.*, 2001]) data, balloon-borne soundings, and satellite retrievals over the ARM SCF, it is possible to develop a better understanding of the relationship between measured and modeled meteorological state parameters and the cloud properties in a given volume of air in many different conditions. With the ARSCL cloud product, it is possible to definitively study the dependence of cloud cover on RH and vertical wind and develop a more reliable method for estimating cloud occurrence.

[8] Another important relationship is the distribution law of the relative humidity in the upper troposphere and lower stratosphere. The role of upper tropospheric humidity (UTH) in the climate system is much less clear than it is in the lower troposphere. *Lindzen* [1990] and *Pierrehumbert* [1994] discussed possible mechanisms that lead to a decrease of UTH in response to global warming. This might reduce or even reverse the water vapor feedback. On the other hand, *Rind et al.* [1991] argued for moistening of the upper troposphere as a result of global warming. Unfortunately, the water vapor content of the upper troposphere is not well known [e.g., *Minnis et al.*, 2004b]. Operational radiosondes, which furnish a wealth of humidity data from the lower and middle troposphere, tend to have no response or yield dry-biased measurements in the upper troposphere [*Gierens et al.*, 1999; *Miloshevich et al.*, 2001; *Wang et al.*, 2003]. High supersaturations with respect to ice are a prerequisite for the formation of cirrus clouds and persistent spreading contrails [*Gierens*, 1996; *Minnis et al.*, 2004b]. A significant portion of the upper troposphere, however, is supersaturated with respect to ice but is cloud free [*Spichtinger et al.*, 2003]. This variable volume of clear air represents the potential for an increase in cirrus coverage that would result from high-altitude air traffic and affect the climate [*Minnis et al.*, 2004b]. Thus, more accurate knowledge of the dependence of cloud cover on UTH as measured or modeled would make it possible to better predict when and where air traffic is likely to produce more cirrus clouds through contrail formation. Soundings by themselves do not provide sufficient information to distinguish between cloudy and cloud-free parts of the profile. With the ARM ARSCL measurements, it is possible to detect cloud–free ice-supersaturated layers in either measured or modeled humidity fields and to study the RH distribution law for cloudy and clear layers.

[9] In this study, the relationships and differences between modeled and ARM-measured meteorological state parameters in clear and cloudy conditions are studied and used to develop a temperature and vertical velocity dependent RH threshold cloud detection method. The model used here is the RUC, a high-resolution, state-of-the-art numerical weather analysis. The differences between the radiosonde and model results should be representative of how accurately cloud structure can be defined by such models and provide a basis for improving the cloud parameterizations used in those models. Additionally, the frequency of occurrence and statistical properties of cloud-free ice-supersaturated and subsaturated layers in the upper troposphere are also investigated using the same data to better determine the potential for cirrus and contrail formation. By combining numerical weather forecasts or analyses with satellite data, it might be possible to continuously unscramble the vertical structure of clouds in either real time or post facto, to improve subsequent forecasts through assimilation of the combined results, and to improve diagnoses of other valuable parameters such as aircraft icing potential for cloud layers beneath satellite-observed high-level ice clouds.

2. Data

[10] The modeled atmospheric profiles of height, temperature, relative humidity, and horizontal and vertical wind speeds were derived from the 40-km resolution, 1-hourly Rapid Update Cycle (RUC-2) analyses [*Benjamin et al.*, 1998] in 25-hPa intervals from the surface to 100 hPa. The values at the RUC grid point closest to the SCF (36.617°N, 97.5°W) were used in this study. The RUC-2 (see http://maps.fsl.noaa.gov/ruc2.tpb.html# Data for more details) was upgraded to a 20-km resolution model (RUC20) in April 2002 [*Benjamin et al.*, 2004a, 2004b] to accommodate a change in the ice cloud microphysical parameterization that will affect some of the results at high altitudes. This study uses data from the RUC-2 period because of the availability of ARSCL products. Unless otherwise indicated, hereafter, RUC is synonymous with RUC-2. The RUC also produces a diagnosis of hydrometeor content, a subject for comparison in a future study. Validation of forecasts is not part of this study, therefore, only RUC analyses are used here instead of forecasts.

[11] The RUC assimilates vertical profiles of temperature, humidity, and wind from rawinsonde, aircraft, and wind profilers at all available locations. The nearest operational rawinsonde stations are in Dodge City, Kansas (uses Sippican VIS-B2 radiosondes) and Norman, Oklahoma (uses Vaisala RS80-H radiosondes). Although the ARM SCF rawinsonde data are currently assimilated by the RUC, it is uncertain whether they were included in the RUC data stream during the period under study here. The satellite-derived cloud-drift winds and precipitable water retrievals are assimilated over water-surface points. Cloud condensate, predicted explicitly from the previous hour's RUC forecast using a cloud physics package, is used to initialize each model run to avoid cloud spin-up problems. No cloud observations are used.

[12] Radiosonde (SONDE) data collected at the SCF with Vaisala RS80-15LH radiosondes from 1 March 2000 to 28 February 2001 were used as the best available atmospheric profiles. Normally, four radiosondes are launched every 6 hours each day beginning at 0000 UTC. During ARM Intensive Operation Periods, which typically occur 3–5 times per year, radiosondes are launched 8 times

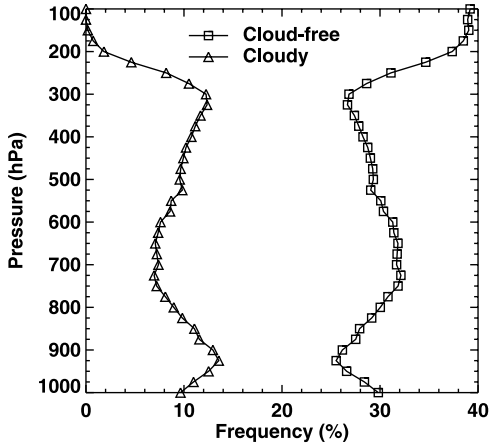

Figure 1. Vertical distribution of the occurrence frequency of cloudy and cloud-free layers in cloudy-sky soundings relative to the total number of profiles. The frequency of the clear sky cases (not shown) examined was 60%.

per day at the SCF. They provide high-resolution profiles of pressure, temperature, relative humidity with respect to liquid water, and wind speed and direction. The reported values cover the pressure range from the surface to the maximum observation level. No corrections were applied to the SONDE data.

[13] To reduce RH measurement noise and facilitate processing, the radiosonde profiles were vertically smoothed into 25-hPa intervals from the surface to 100 hPa. The time of the sounding midpoint was determined for each radiosonde ascent and matched with the closest hourly RUC analysis profile. The relative humidities from both SONDE and RUC data are defined with respect to liquid water (RHW) at all temperatures and converted to RH with respect to ice (RHI) at temperatures less than or equal to 253 K, the midpoint between the freezing point and the homogeneous ice nucleation point. Unless otherwise noted, hereafter, RH will be used synonymously with that temperature-dependent definition. The mean RH was computed for each layer by averaging the relative humidities at the top and bottom of each layer.

[14] The ARSCL cloud product consists of cloud base and top heights for each 10-second interval using the algorithms of *Clothiaux et al.* [2000] with a combination of Belfort Laser Ceilometer, MMCR, and Micropulse Lidar data. The cloud base and top heights used in this study are 10-min averages centered on the RUC times. In a given measurement interval, a layer is classified as cloudy if any portion of the cloud occurred within the layer. *Clothiaux et al.* [2001] provide a detailed description of the ARSCL data set. Their approach requires the advection of clouds over the point to estimate, essentially, the cloud fraction over a line. It is assumed in the comparisons that this cloud fraction corresponds to that for the same 40-km area of the RUC grid and to that volume of space determined by the flight path of the radiosonde.

[15] Generally, the ARSCL instruments and algorithm yield very accurate definitions of cloud boundaries, but errors in the data products can arise for a variety of reasons. During warm months, analysis of the MMCR return can, at times, confuse clutter such as insects or vegetation debris as cloud droplets up to altitudes as high as 5 km despite efforts to eliminate the false returns. Since the MPL and ceilometer cannot penetrate through thick clouds, the cloud top boundary for such clouds is entirely dependent on the MMCR. Some clouds and parts of clouds containing small particles may not produce a radar return causing the cloud or a portion of it to be missed especially if the cloud is at high altitudes where the return is weaker. These two error sources, therefore, can cause an underestimate of cloud base heights at low levels and cloud top heights at higher levels. Other sources of error in cloud boundaries determined from combined MPL, MMCR, and ceilometer data are discussed by *Naud et al.* [2003].

3. Results

[16] The combined data set consists of 1150 SONDE soundings matched with RUC profiles and ARSCL cloud boundary data. Each layer in the SONDE and RUC data is identified as a cloud-free or cloudy layer using ARSCL cloud boundary data. If all layers are cloud-free for a given profile, then it is defined as a clear-sky sounding, otherwise, as a cloudy-sky sounding. Approximately 60% of these soundings or RUC profiles are classified as clear-sky soundings with the remaining 40% classified as cloudy-sky soundings.

3.1. Comparison of SONDE and RUC Data

[17] Figure 1 shows the vertical distribution of the percentage of cloudy and cloud-free layers in cloudy-sky soundings relative to the total number of soundings. From the surface up to 100 hPa, the frequency of cloud layer occurrence is less than 14%. The maximum occurrences of cloud layers are in the upper (300 hPa) and lower (975 hPa) troposphere, respectively. Minimum cloud occurrence, 7%, in the troposphere occurs at 725 hPa. Above 300 hPa, the occurrence of cloud-free layers increases dramatically since the tropopause height varies between 100 and 300 hPa.

[18] Relative humidity is a quantity that usually displays a very intricate structure in space and time. Since it depends on both absolute humidity and temperature (T), fluctuations of both these fields translate into relative humidity fluctuations. Figure 2 shows the hourly RUC (thin line) and SONDE (thick line) atmospheric profiles at 2100 UTC, 4 April 2000 (Figure 2a) and 1200 UTC, 3 November 2000 (Figure 2b). The high-cloud layer determined from the ARSCL cloud-base and top heights is illustrated by the gray area. In Figure 2a, both the RUC and SONDE RH's exceed 80% in the cloud layer but are below ice saturation. Outside of the cloud layer, the RUC produces similar RH values over more than 5 km of altitude. In Figure 2b, the SONDE reveals the low-cloud altitude as a spike in RH up to 92%, whereas the RUC is very dry and provides no indication of cloud location. A moist (RH > 90%), in part supersaturated, layer is seen in the SONDE profile between 7 and 12 km. The ARSCL lower cloud boundary roughly coincides with the rise in RH around 6.5 km but it is lower than the decrease in humidity near 12.5 km. Examination of the radar record indicates that the cloud top rose to 12.5 km an hour after these measurements. The moist layer in the SONDE

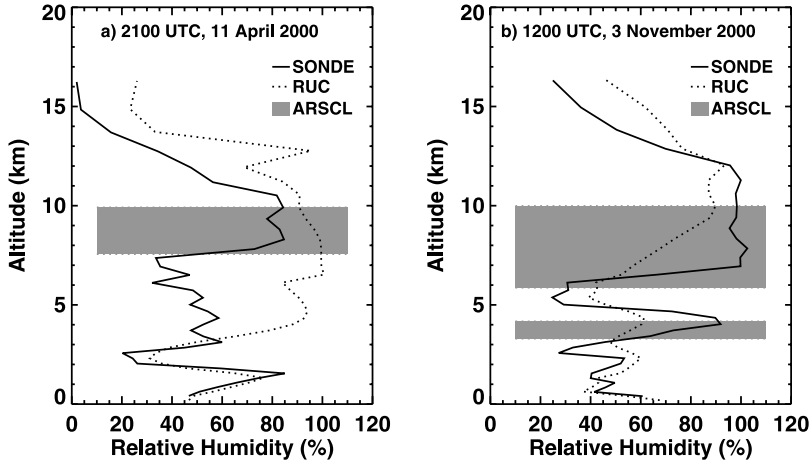

Figure 2. RH profiles from SONDE (thick line) and RUC (thin line) at (a) 2100 UTC, 11 April 2000 and (b) 1200 UTC, 3 November 2000. Gray areas represent cloud layers determined from ARSCL cloud base and top heights.

profile is broader than its RUC counterpart in Figure 2b and has greater values of RH. The SONDE-RUC differences are likely due to smoothing of the fields by the RUC assimilation process.

[19] Figure 3 shows scatterplots of RH and T from SONDE and RUC data in the upper troposphere (250–350 hPa) inside cloudy layers. Both T and RH from the SONDE and RUC profiles are highly correlated but the temperature pairs show much closer correspondence than the RH values. On average, the SONDE RH is greater than that from RUC. This bias may be due to the RUC model constraining humidity values or its use of data from the radiosonde network, which employs a variety of radiosonde models. For example, the VIZ-B sonde used at Dodge City does not respond to humidity changes in the upper troposphere [*Wang et al.*, 2003]. The bias also tends to confirm the absence of ARM SCF soundings in the RUC input data stream. Some RH differences between the RUC and SONDE data are expected since the RH profile actually represents the grid average from RUC analyses, which are based on widely spaced measurements. The radiosonde, being a point measurement, reports the actual instrument-measured atmospheric thermodynamic state if the biases in RH due to instrument errors [*Miloshevich et al.*, 2001; *Wang et al.*, 2002; *Turner et al.*, 2003] are ignored. Thus, the RUC may not reflect or capture some cloud information, especially for short term and small-scale cloud systems.

[20] The SONDE and RUC RH frequency distributions (Figure 4) are distinctly different in clear and cloudy conditions for all layers. The large fluctuations in RH result in highly skewed frequency distributions. The SONDE histograms are more peaked compared to the smoothed RUC data. The two data sets are most similar at the lowest altitudes (highest pressures). Ice-supersaturated layers occur in both cloudy (solid thick lines) and clear layers (solid thin line and line with triangle) in the upper and middle troposphere (100 hPa–700 hPa), but are more common at pressures above 400 hPa. At the highest altitudes, supersaturation occurs in roughly 8% of the SONDE clear layer cases while it is found in 35% of the cloudy cases. These percentages are greater than their RUC counterparts at 6 and 16%, respectively. The SONDE mode values for cloudy layers vary between 95 and 105% depending on the altitude, compared to a range of 75 to 95% for the RUC data. For both data sets at all altitudes, the clear-sky

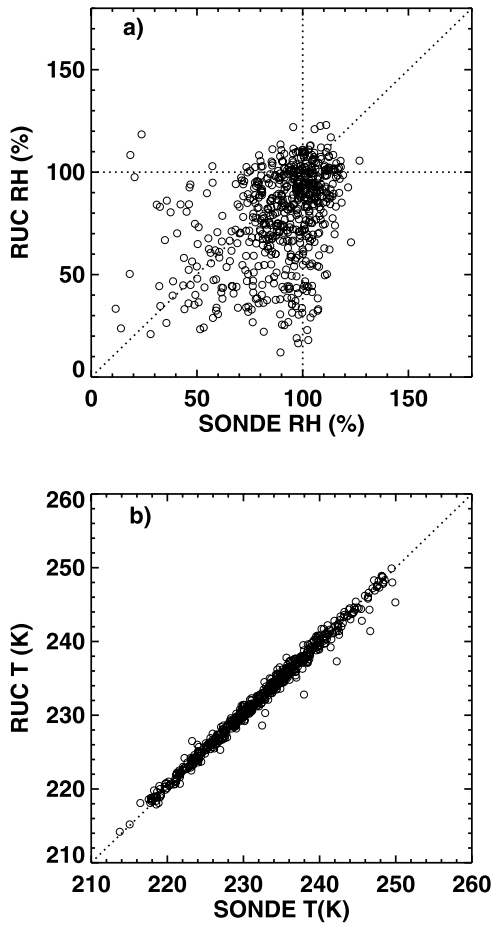

Figure 3. Scatterplots of relative humidity and temperature inside clouds from SONDE and RUC data between 250 and 350 hPa.

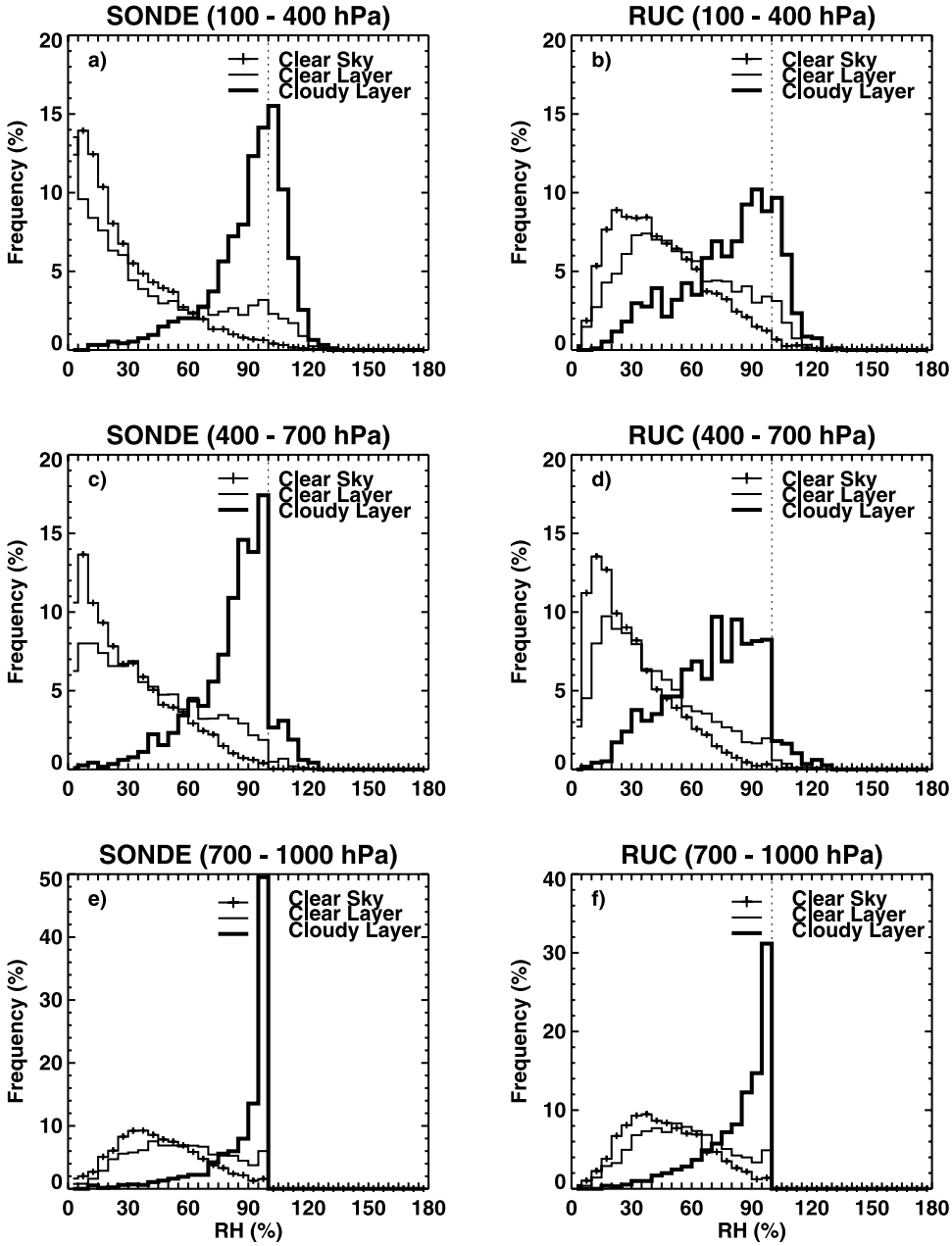

Figure 4. Histograms of the RH from SONDE and RUC in clear and cloudy conditions.

conditions are distinctly drier than the clear layers detected when a cloud occurs within the column (clear layer) suggesting an overall moister atmosphere when a cloud occurs anywhere in the column.

[21] The vertical distributions of the RH and T differences, respectively, between the SONDE and RUC data in clear and cloudy conditions are shown in Figures 5a and 5b along with error bars that indicate the standard error in the estimate of the mean. Inside cloudy layers (thick line), the RH from RUC is 2–14% less than the SONDE values. The differences are statistically different from zero and from the clear and cloud-free cases at all levels above 950 hPa. In contrast, no significant RH differences between the SONDE and RUC data are evident for $p >$ 500 hPa for cloud-free (thin line) or clear-sky (line with circle) layers. At higher altitudes, the RUC is moister in cloud-free and clear-sky conditions than the SONDE with the difference between SONDE and RUC increasing with height (decreasing pressure), especially in the upper troposphere. The RUC contains a sophisticated cloud and moisture scheme that allows for ice supersaturation, a capability lost in the RUC20 formulation. As indicated by Figure 4, though, it computes less supersaturation overall than found with the SONDE data. This finding is consistent with the results of *Duda et al.* [2004], who demonstrated that the RUC underestimates upper tropospheric humidity by showing that persistent contrails developed in regions where the RUC computed an RHI of only 70–85%. On average, the mean RUC temperatures are greater than the SONDE values in all conditions for $p <$ 300 hPa. At altitudes below 500 hPa, the mean temperature differences diverge such that the RUC

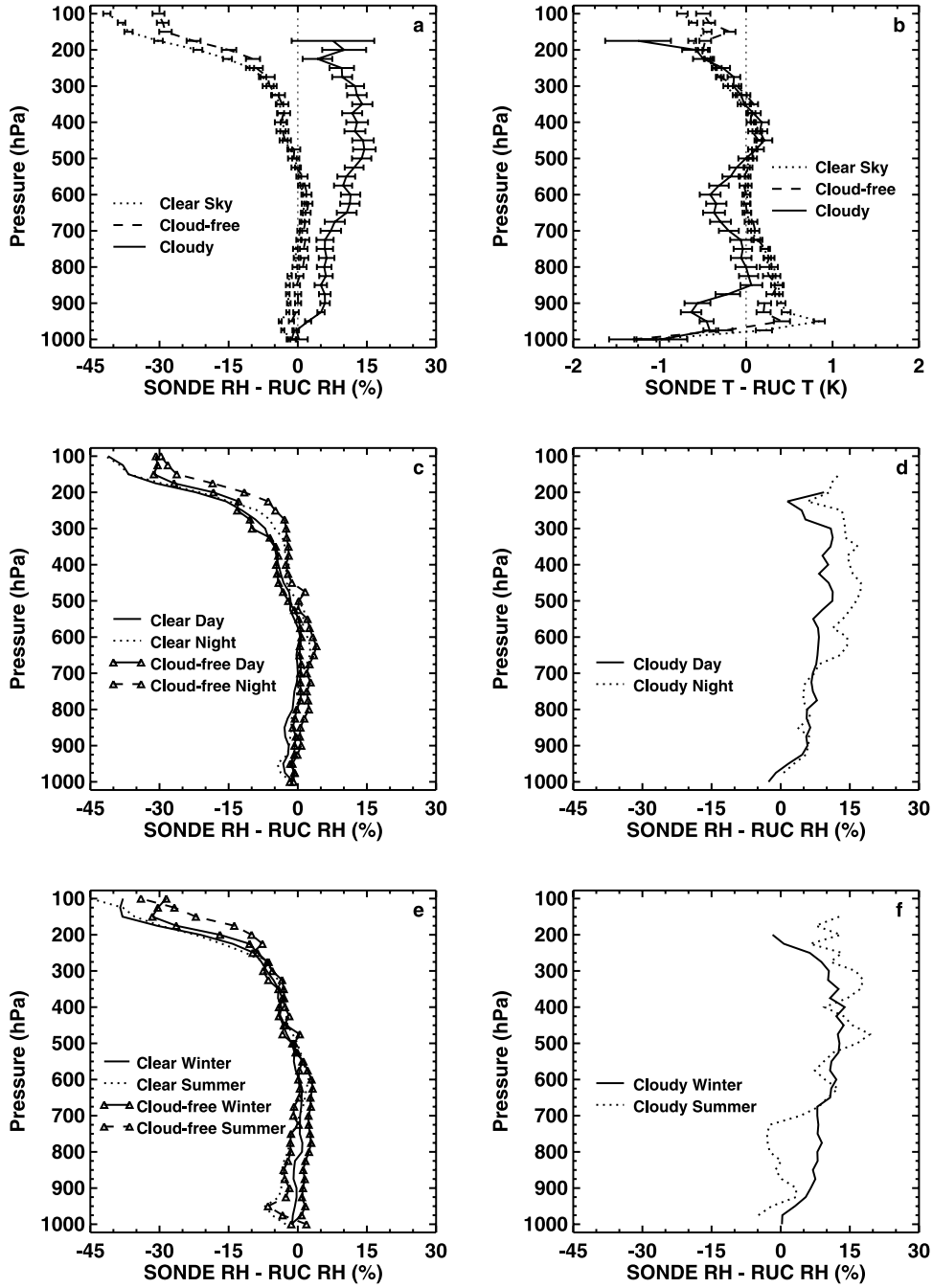

Figure 5. Vertical distributions of (a) RH and (b) T differences between SONDE and RUC data in clear and cloudy conditions and of (c, d) diurnal and (e, f) seasonal SONDE-RUC RH differences for clear and cloud-free conditions and for cloudy layers. Error bars indicate standard estimate of the error in the mean for each layer.

tends to be warmer in cloudy layers and colder in clear layers.

[22] The RH differences for clear and cloud-free conditions differ little between day and night for $p > 700$ hPa, but at higher altitudes, the SONDE tends to be systematically moister at night by up 7% (Figure 5c). This diurnal difference is even more marked for the cloudy cases suggesting that the RUC tends to produce more drying at night above the boundary layer than during the daytime. The RUC produces a slightly moister boundary layer than the SONDE in clear and cloud-free conditions during summer (Figure 3e), while during winter, the mean SONDE and RUC RH values are nearly identical for $p > 500$ hPa. Seasonal changes at lower pressures are minor. In cloudy conditions (Figure 3f), the mean RUC and SONDE boundary layer humidities are nearly identical during summer, but the RUC boundary layer is drier than the SONDE during winter. At higher

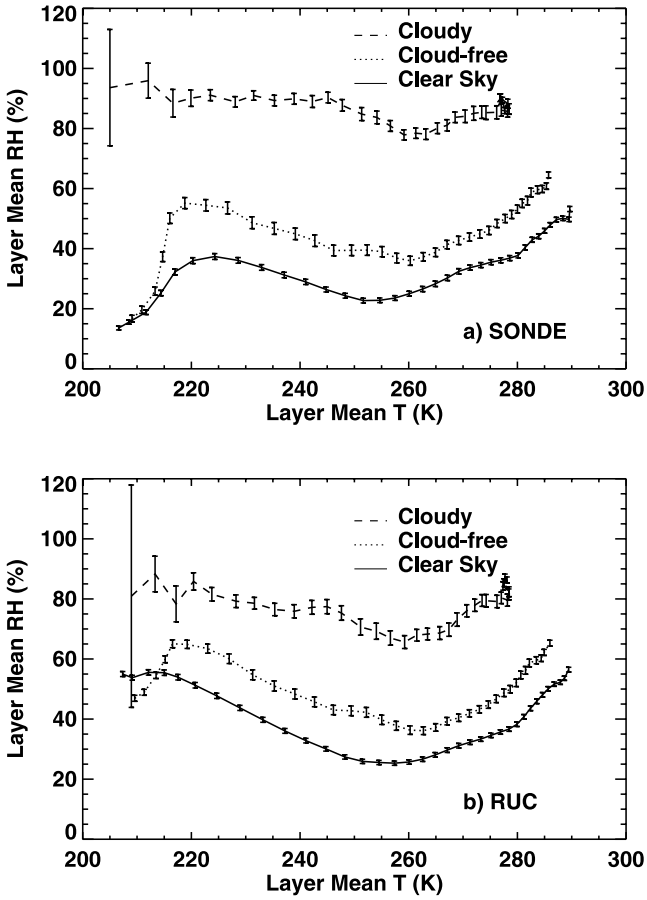

Figure 6. Variations of (a) SONDE and (b) RUC layer mean RH with the layer mean temperature for clear and cloudy conditions. Error bars indicate standard estimate of the error in the mean for each temperature.

altitudes, the seasonal variation in the RH differences is minor.

3.2. Variation of RH With Temperature for Clear and Cloudy Layers

[23] The variations of the SONDE and RUC layer mean RH with the layer mean temperatures are shown in Figure 6 for clear and cloudy conditions along with error bars indicating the standard error in the estimate of the mean for each layer. Differences between the means for all three categories are statistically significant for both data sets, except for T < 215 K. The impact of the arbitrary selection of T = 253 K for a switch from RH to RHI is evident in the RH minima around 255–260 K. Although the layer mean RH inside clouds is well separated from layer mean RH in clear conditions, it is evident that RH thresholds chosen as a function of temperature should more accurately diagnose cloud occurrence than the assumption of a fixed RH threshold.

[24] To develop relationships between RH and cloud probability as functions of temperature, frequency distributions of RH were constructed for each temperature interval. Figure 7 shows the frequency distributions of RH when the ambient temperature is between 250 and 254 K. The histograms (solid lines) and Gaussian fits (dotted lines) are presented together in Figures 7a and 7b for the SONDE and RUC data, respectively. The blue solid and dotted lines show that the histogram and Gaussian fit are in relatively good agreement, which indicates that the relative humidity inside cloudy layers can be described by a Gaussian (normal) distribution. As in Figure 4 for high clouds, the RUC histogram in Figure 7 is much broader than its SONDE counterpart. Outside of cloudy layers (red) and in clear-sky conditions (green), however, RH is not adequately represented by a normal distribution but might be represented better using an exponential distribution (see section 4.3 below). *Ovarlez et al.* [2002] also found that the RH statistics outside and inside of clouds are fundamentally different: the relative humidity within clouds is better described by either a Gaussian or a Rayleigh distribution centered at the saturation point. The cumulative distribution functions (Figures 7c and 7d) reveal that when RH < 67.5% for SONDE and 48.4% for RUC, the probability of finding a cloud is 20%. In other words, the RH threshold value, with 20% probability of finding a cloud, is 67.5% for the SONDE and 48.4% for the RUC. Similarly, the RH thresholds can be determined for different probabilities (40%, 60%, and 80%) of finding a cloud as shown in Table 1.

[25] The frequency of cloud occurrence for a given RH value and T interval was determined by repeating the above procedures for other temperature ranges. The two-dimensional frequency distributions of cloud occurrence for both SONDE and RUC data are shown in Figure 8. The RH threshold values used to diagnose different cloud probabilities for the SONDE and RUC data are shown as thin gray lines in Figures 8a and 8b, respectively. As indicated earlier, the dip in the contours around 255 K is due to the switch from RHW to RHI. When $T < 245$ K, the RH thresholds vary little with temperature. For a given cloud probability, the SONDE RH thresholds are greater than their RUC counterparts, except for smaller probabilities in warmer air ($T >$ 284 K). The thresholds decrease with increasing temperature for warm clouds, perhaps reflecting differences in cloud dynamics, i.e., stratus versus cumulus clouds. Some of the extreme points in the lower right corner of the plots may be due to aerosols misclassified as clouds in the ARSCL data or to errors in the RH.

[26] To determine the value of these thresholds, each layer in the RH profiles from both data sets is classified as being clear or cloudy. A layer with RH equal to or exceeding the threshold values from Figure 8 is identified as a cloudy layer (Rcld). A layer having RH below the thresholds is determined to be a clear layer (Rclr). Table 2 lists the percentages of matched clear and cloudy layers for both SONDE and RUC for five probabilities of detecting a cloud. Matched cases consist of layers identified as either cloudy or cloud-free by both ARSCL and the RH thresholds. Mismatched cases are those in which the layers identified as clear or cloudy by ARSCL are identified as cloudy or clear, respectively, by the RH threshold method. The RUC and SONDE results are similar for the matched clear cases in that differences in agreement for the clear cases are no greater than 6%. The levels of agreement are worse for the cloudy cases.

[27] So far, only overcast conditions have been considered, that is, the ARSCL cloud amount is over 90%. The ARSCL cloud amount is computed as the frequency of cloud occurrence for each 10-second interval during a 10-minute period. For example, if a cloud occurrence is recorded

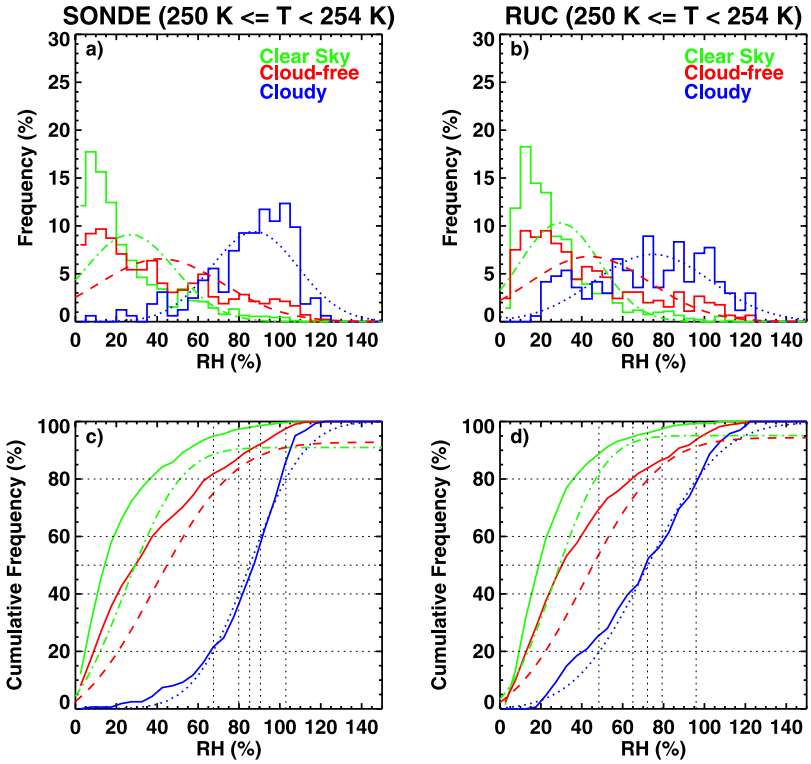

Figure 7. Frequency distributions of relative humidity from all cloud layers where the ambient temperature is greater than 250 K and less than 254 K, for both SONDE and RUC data.

for half of the 10-second measurements within a given 10-minute period, the ARSCL cloud amount is defined as 50%. To study the variation of cloud fraction with RH, the RHs are divided into three groups according to the ARSCL cloud amount, i.e., 10%–30%, 30%–60%, and 60%–90%, respectively. In each group, the RH frequency distributions (not shown) were examined for two different temperature regimes, that is, T > 253 K or T < 253 K, to determine the probability thresholds. As seen in Figure 9, the resulting RH thresholds increase monotonically with cloud amount for all cases except P20 for warm clouds. The thresholds increase at a lower rate for ice clouds (Figure 9a) than for liquid clouds (Figure 9b). Generally, the difference in RH thresholds between the SONDE and RUC RH thresholds is smaller in partly cloudy than in overcast conditions, especially for ice clouds. Additionally, while the RUC probabilities change almost linearly with cloud amount between 20 and 100%, the SONDE overcast probabilities for ice clouds represent a marked departure from the otherwise linear changes for partly cloudy conditions. From these results, a RUC or SONDE sounding could be used to estimate both the probability of a particular cloud amount at a given level in the atmosphere. For example, in Figure 9a at RH = 70% the probability of finding an overcast cloud is ~20% while the probability of finding 20% cloud cover is 50%. Hereafter, only the overcast probabilities are considered.

3.3. Variation of Cloud Probability With Layer Vertical Velocity

[28] The vertical distributions of the RUC layer mean vertical velocity, expressed as omega ω (hPa s^{-1}), in clear and cloudy conditions are shown in Figure 10 along with the standard errors of the estimate of the means. On average, the vertical motion inside the cloud layers is dominated by upward motion (negative values) whereas cloud-free layers have almost no mean vertical motion except in the lower troposphere (<700 hPa). The difference between cloudy and clear-sky vertical velocity is significant in all RUC layers except the boundary layer. The maximum difference is in the middle troposphere (400–700 hPa). Downward motion dominates the clear-sky condition for pressures less than 825 hPa. Figure 10 also reveals that the upward motion is very weak in the cloudy upper troposphere between 200 and 400 hPa. This result suggests that only a very small uplift is required for cirrus formation.

[29] Mean values of ω were also computed separately for daytime and nighttime yielding only minor differences (not shown). No significant day-night differences in the mean vertical velocities were seen for p < 350 hPa for any category. Between 350 and 800 hPa, ω was 0.1 hPa s^{-1} greater at night than during the day for clear skies. For p > 800 hPa, the difference was reversed. No significant diurnal differences were seen at any level for the cloud-free and cloudy categories.

Table 1. RH Threshold Values for SONDE and RUC at Different Probabilities of Finding a Cloud When the Temperature is Between 250 K and 254 K

RH, %	P20	P40	P50	P60	P80
SONDE	67.52	79.88	85.22	90.56	102.92
RUC	48.37	64.98	72.14	79.30	95.92

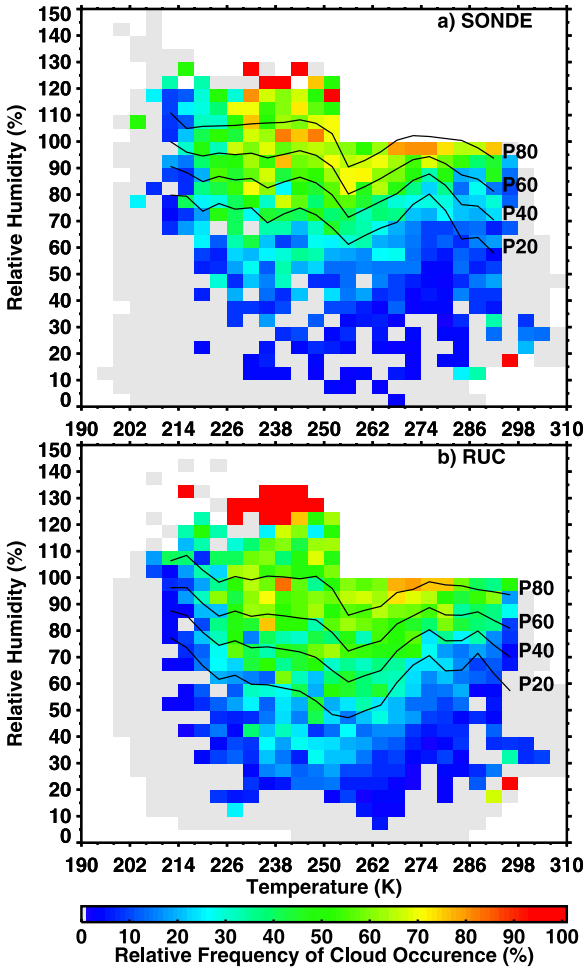

Figure 8. Two-dimensional frequency distribution of cloud occurrence for a given RH and T for both SONDE and RUC.

[30] The probability thresholds for clouds as a function of temperature and vertical velocity are plotted in Figure 11. The P20 values are relatively constant at ~0.15 hPa s^{-1}, while the remaining curves show a substantial variation with temperature. In the upper troposphere ($T < 230$ K), the range in ω between P20 and P80 is less than 0.2 hPa s^{-1}, confirming the idea that small changes in uplift have a large impact on cirrus maintenance. The range increases to more than 0.6 hPa s^{-1} at T = 287 K before dropping again at higher temperatures. Thus, a given change in vertical velocity has much less influence in the lower troposphere than at higher altitudes.

3.4. Parameterization of Cloud Probability

[31] The influences of temperature, humidity, and vertical velocity on cloud probability are related to each other. For example, stronger upward motion results in a moister layer. To optimally estimate the probability, P_{cld}, of finding a cloud in a given layer, all three variables should be considered together. Using RH in %, T in K, and ω in hPa s^{-1}, an empirical model is developed using the Gaussian distributions derived from the RUC and SONDE data using only the overcast (cld > 90%) data. This model is formulated as follows.

$$P_{cld} = P_R(T, RH) + f(\omega), \tag{1}$$

where

$$P_R(T, RH) = A_0 + A_1 e^{-\frac{[\zeta_1(T,RH)]^2 + [\zeta_2(T,RH)]^2}{2}}, \tag{2}$$

$$\zeta_1(T, RH) = [(T - b_1)\cos b_2 - (RH - b_3)\sin b_2]b_4/b_5, \tag{3}$$

$$\zeta_2(T, RH) = [(T - b_1)\sin b_2 + (RH - b_3)\cos b_2]/b_6. \tag{4}$$

Also, if T > 250 K,

$$f(\omega) = -2.366 - 16.51\omega. \tag{5}$$

Otherwise, $f(\omega) = 0$. Since vertical velocity is not available for the SONDE data, (1) reduces to

$$P_{cld}(T, RH, \omega) = P_R(T, RH). \tag{6}$$

[32] Equations (1) and (6) were fitted to the RUC and SONDE overcast data, respectively, resulting in values for each of the coefficient sets, $\{A_i, i = 0, 1\}$ and $\{\{b_i, i = 1, 6\}$, listed in Table 3. Relative humidity is the most important factor for cloud formation (e.g., Figure 4), so it is given most of the influence in the above parameterization. The impact of vertical velocity is less distinct (Figure 11) so it is only used to modify the RH-based probabilities. The coefficients for equation (5) were derived from the RUC data for $T > 250$ K. No attempt was made to account for the vertical velocity for lower temperatures (higher altitudes) because the impact is negligible. In application, P_{cld} is constrained to values between 0 and 100%.

Table 2. Percentage of Matched and Mismatched Layers in Clear and Cloud Conditions for Both SONDE and RUC[a]

	Aclr → Rclr		Acld → Rcld		Aclr → Rcld		Acld → Rclr	
	SONDE	RUC	SONDE	RUC	SONDE	RUC	SONDE	RUC
P20	85.7	79.2	82.7	79.3	14.26	20.81	17.27	20.73
P40	91.6	88.3	71.9	65.2	8.44	11.73	28.10	34.76
P50	93.5	91.3	64.2	58.2	6.50	8.65	35.77	41.79
P60	95.4	93.7	53.9	49.6	4.64	6.26	46.10	50.38
P80	98.9	97.8	10.1	23.4	1.12	2.17	89.85	76.63

[a]Aclr, ARSCL clear layer; Acld, ARSCL cloud layer. Rclr, clear layer determined by the RH threshold method; Rcld, cloudy layer determined by the RH threshold method.

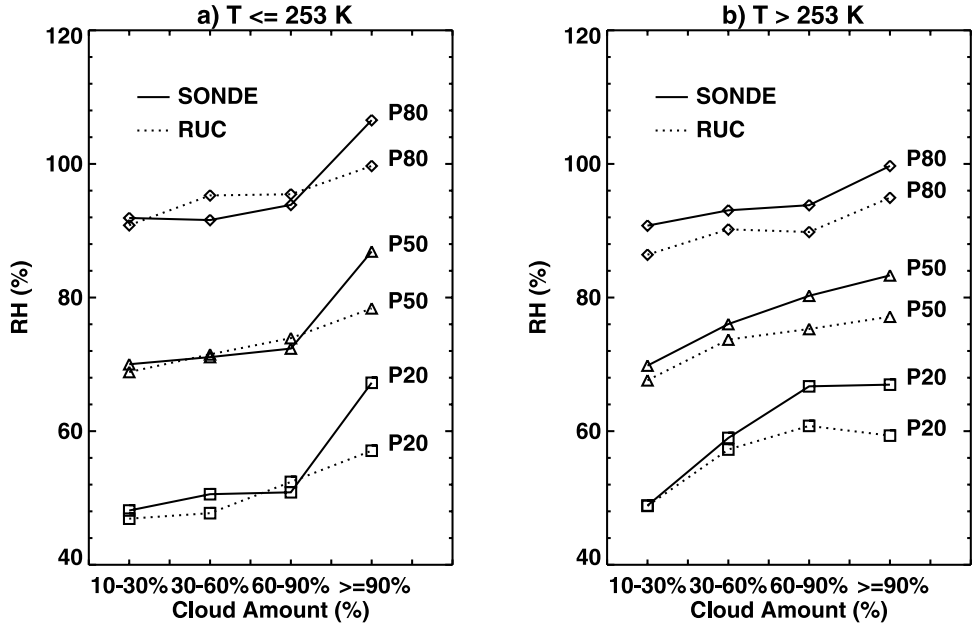

Figure 9. Variation of the RH thresholds with cloud amount for (a) ice cloud, $T \leq 253$ K and (b) water cloud, $T > 253$ K.

[33] Figure 12 shows examples of the parameterization for two temperatures. The RUC probabilities for a given RH exceed their SONDE counterparts by as much as 20% as a result of the greater values of SONDE RH in a given cloud layer (Figure 5a). Between 220 K and 280 K, the probability for having an overcast cloud layer is nearly identical between RH values of 50 and 80% for the SONDE data and between 30 and 60% for the RUC data. The probabilities diverge at larger values of RH with lower probabilities at lower temperatures. This temperature dependence arises in part from the relatively frequent occurrence of cloud-free ice-supersaturated layers and the requirement for large supersaturations to form ice clouds. The probability for cloud formation does not reach 100% at 280 K for the RH(SONDE) = 100% because of the occasional mismatch between location of the cloud and the humidity as seen in the occurrence of some clear layers with RH = 100% in Figure 4. Additionally, the use of the normal distribution for the cloudy RH does not capture the extreme skewness of the actual probability distributions. Nevertheless, the model produces the essential elements of the relationships between T and RH seen in Figure 4. Varying the vertical velocity between -0.3 and 0.1 hPa s^{-1} alters the probabilities for the 280-K case between 2.6 and -4.0%, respectively. Presumably, the models formulated in Equations (1) and (6) could be scaled to assess the probabilities for particular cloud fractions using data like those in Figure 9. For example, for the 220-K overcast case in Figure 9a, the 50% probability for a cloud amount of 45% at T = 220 K would correspond to RH = 73% or roughly to P_{cld} = 43% in Figure 12.

4. Discussion

4.1. Gridding, Layer, and Sampling Errors

[34] The analyses presented above only approximate the true probabilistic relationships between clouds and humidity for several reasons. Discretization, which arises whenever a regular grid is imposed on a natural process, diminishes the one-to-one correspondence between the cloud and the relative humidity. The definition of the cloud cover does not require filling the entire depth of a 25-hPa layer. Thus, a thin cloud may only occupy a depth of 5 or 10 hPa in some stable sublayer within the 25-hPa layer, yet the presence of the cloud is associated with the layer mean RH, which is likely to be diluted relative to the sublayer RH. This dilution effect can help explain the broadening of the humidity range for the cloudy layers (Figure 4), even for the SONDE measurements. In addition to thin clouds that do not vertically extend throughout a layer, many thicker clouds

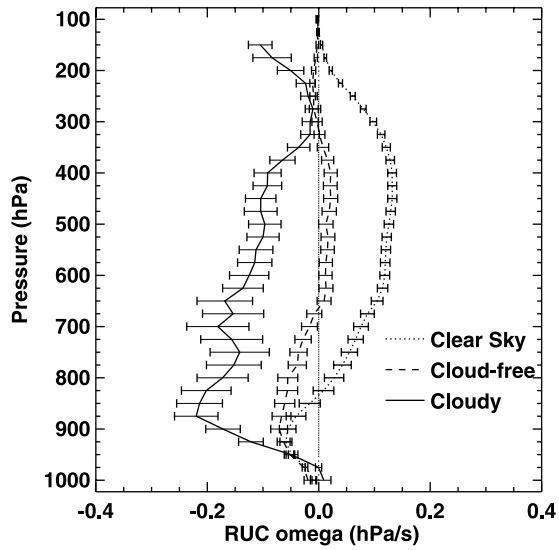

Figure 10. Vertical distribution of layer mean vertical motion (negative, upward motion) in clear and cloudy conditions. Error bars indicate standard estimate of the error in the mean for each layer.

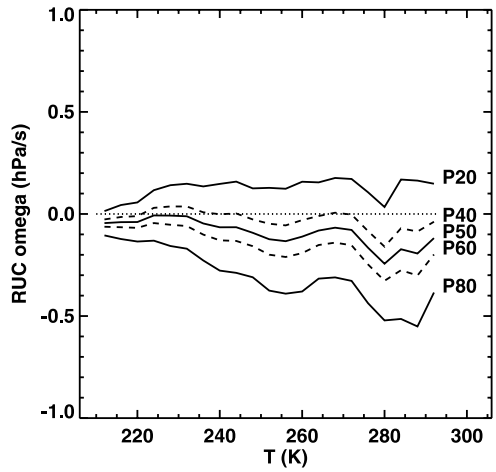

Figure 11. Vertical velocity threshold values for RUC at different probabilities of finding a cloudy layer.

will cross grid boundaries resulting in the top or bottom of the cloud filling only a portion of their respective layers. Conversely, the true cloud-layer RH can be diluted by using the discrete levels to compute RH in both data sets. Furthermore, because the SONDE requires more than 30 min to ascend through the troposphere (at an ascent rate of 5 m/s), it could pass through breaks in the clouds yielding humidities that are less than those in the cloudy parts of the layer. Thus, the RH values corresponding to actual clouds would generally be greater than those found here.

[35] At low and middle levels, the RUC yields distributions of RH that are similar to those from the SONDE data for clear and cloudy conditions (Figure 4), while the RH thresholds are less than their SONDE counterparts for a given value of P_{cld}. This difference results from the discrepancies in the cloud layer distributions. The greater peaks in the SONDE distributions for layers between 400 and 1000 hPa, indeed at all levels, result from a better match between the moisture and cloud layer in the SONDE profiles as exemplified by the plots in Figure 2. The model might have the necessary level of humidity, but it does not always place it at the proper altitude resulting in a spreading of the cloudy layer histogram. This spreading forces the RUC thresholds to lower values of RH for a given probability. Another factor in the lower values of RUC RH for a given threshold is an apparent dry bias in the RUC relative to the SONDE data as seen in Figure 5. Some of the bias may be due to differences in the operational and ARM radiosondes, but some of it could be due to some drying of the troposphere by the assimilation process.

[36] Other sources of error are the differences in spatial and temporal sampling. The ARSCL provides only a linear sample of clouds in the area covered by the RUC and that sample is not likely to coincide with the path of the radiosonde. Thus, RUC and SONDE areas classified as clear by the ARSCL could contain clouds while the ARSCL overcast scenes could have clear areas that were not sampled by the advection process needed for the ARSCL cloud fraction calculations. *Nordeen et al.* [2005] compared ARSCL cloud fractions with those estimated from satellite and total-sky imager (TSI) data, which provide estimates of cloud amount over contiguous areas similar in size to the RUC grid. They found that 90% of the time the ARSCL and satellite results were in agreement for clear conditions and 84% of the time for overcast scenes. The agreement was worse for partly and mostly cloudy scenes. On the whole, the ARSCL tended to underestimate cloud fraction relative to both the satellite and TSI observations over the SCF. Thus, the RH thresholds derived here may be too large. Nevertheless, the comparisons indicate that the ARSCL cloud amounts provide a relatively accurate representation of total cloud fraction most of the time.

[37] The systematic seasonal and diurnal changes between the RUC and SONDE RH differences (Figures 5c–5f) indicate that the thresholds for detecting cloud cover in the RUC and, possibly, the SONDE data could be refined further to account for the systematic temporal variations. Development of more sophisticated thresholds would require much more data than available for this study and, therefore, is beyond the scope of this paper.

4.2. SONDE and RUC Dry Bias

[38] The RH values corresponding to clouds, especially those in the ice phase, may be lower than expected because of biases in the soundings due to aging of the sensor, slow sensor response at low temperatures, and temperature dependence of the sensor response. The offsets between the ARSCL cloud boundaries and maximum SONDE humidities in Figure 2 illustrate the time lag effect while the relatively low values of RH in the cloud layer serve as an example of the sensor's dry bias, which is worse at low temperatures. The ARM program used the Vaisala RS80-15LH with the H-Humicap sensor as its only radiosonde from its beginning in 1992 until April 2001. *Miloshevich et al.* [2004] reviewed the various sources of error in humidity measured with the Humicap sensor and provide a set of correction formulae to reduce the errors to ±2% RH at all temperatures relative to a balloon-borne cryogenic hygrometer. Without those corrections, the underestimate ranges from 4% RH at −20°C to 10% at −70°C. For SONDES older than 0.5 years, the errors can be much larger. Thus, the SONDE probability thresholds would be correspondingly higher if corrections had been applied to the SONDE results.

[39] Presumably, the RUC suffers from a similar type of bias because its humidities are originally based on radiosonde data. Since the US radiosonde network uses a variety

Table 3. Coefficients for Equations (1)–(6)

	A_0	A_1	b_1	b_2	b_3	b_4	b_5	b_6
RUC T > 253	2.384	113.1	237.6	−0.191	110.4	0.0	1.0	30.46
RUC T < 253	−1.355	106.8	209.2	−1.090	134.2	1.0	34.76	−105.5
SONDE T > 253	2.953	157.3	266.1	−0.419	127.3	1.0	−48.68	27.49
SONDE T < 253	−0.518	102.8	240.0	1.633	122.8	1.0	29.59	−170.1

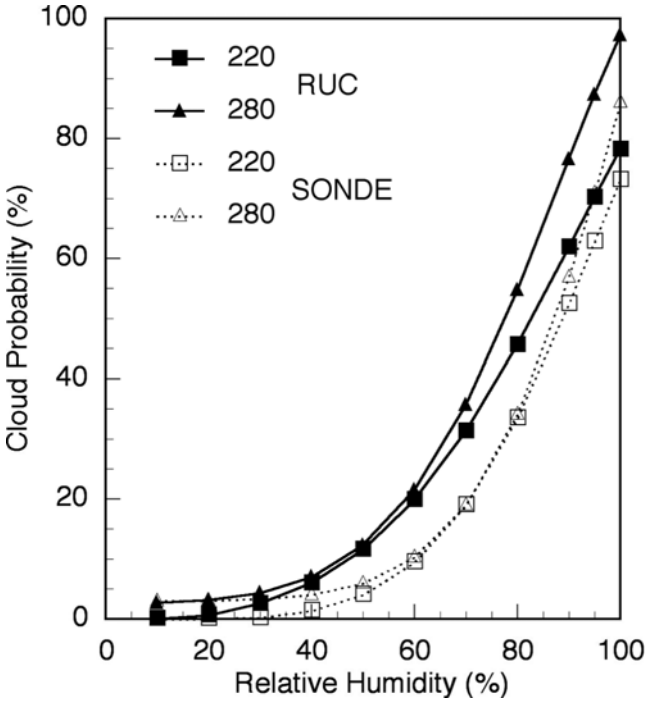

Figure 12. Variation of cloud occurrence probability from parameterization fits to RUC and SONDE RH data at 220 and 280 K.

of sensors with unknown corrections for each sensor, the data assimilated by the RUC are not corrected for aging of the sonde (Vaisala sondes manufactured after May 2001 are not subject to the aging problems of earlier models), time lags, or temperature dependence. The lower RH threshold for the RUC probabilities compared to the SONDE data at low temperatures probably reflects the use of some Vaisala RS80-A and Sippican VIZ-B radiosondes in the operational data set. The RS80-A has a larger temperature-dependent bias than the RS80-H. As noted earlier, the VIZ-B sondes are unresponsive to RH changes in the upper troposphere. No correction is applied to account for either bias errors, so they would be assimilated into the RUC model. As long as corrected radiosonde RH profiles are not assimilated into the RUC, the cloud probability thresholds formulated here should be applicable to the RUC data. The greater dry bias in the operational data at the lower temperatures does not account for the bias seen at low altitudes (Figure 5a). The temperature differences in Figure 5b account for less than 1% of the RH difference at all altitudes. Therefore, it is concluded that some additional drying occurs in the RUC assimilation process.

4.3. Upper Tropospheric Cloud Relationships

[40] From Figures 4 and 10, it is clear that cloud-free ice supersaturated air occurs in clear sky and cloud-free layers as well as in cloudy layers. Given the dry biases in both the RUC and SONDE data and the common occurrence of persistent contrails in apparent subsaturated conditions [*Sassen*, 1997; *Minnis et al.*, 2003], the true frequency of both cloudy and cloud-free supersaturated layers is greater than indicated in those figures. The empirical thresholds can be used to account for the biases in estimating cloud potential, but it is not clear if the RUC produces a realistic distribution of clear and cloud free ice-supersaturated conditions. *Spichtinger et al.* [2002, 2003] used data from the Microwave Limb Sounder (MLS) on board the Upper Atmospheric Research Satellite (UARS) and data from corrected Vaisala RS80-A operational radiosondes to study the humidity statistics inside and outside of ice-supersaturated layers. They found that the probability of measuring a certain RHI, in the subsaturated and the supersaturated tropospheric layers, respectively, decreases exponentially with the relative humidity but with different slopes.

[41] The distributions of the number of upper tropospheric layers having RH within each 2% RH interval are shown in Figure 13. The separated exponential fits are adapted for RH above and below 100%. The slope of the exponential (Table 4) is steeper for the RUC than for the SONDE data. A break in the exponential distribution occurs around RH = 100%, indicating the onset of ice formation. The exponential distribution of supersaturation for RH > 100% is characteristic of ice supersaturated layers. This exponential distribution is also found for RH > 10% (SONDE) and RH > 20% (RUC) in tropospheric subsaturated regions but with a flatter slope than in supersaturated layers (Table 4). The 50% probabilities for finding a cloud within a layer

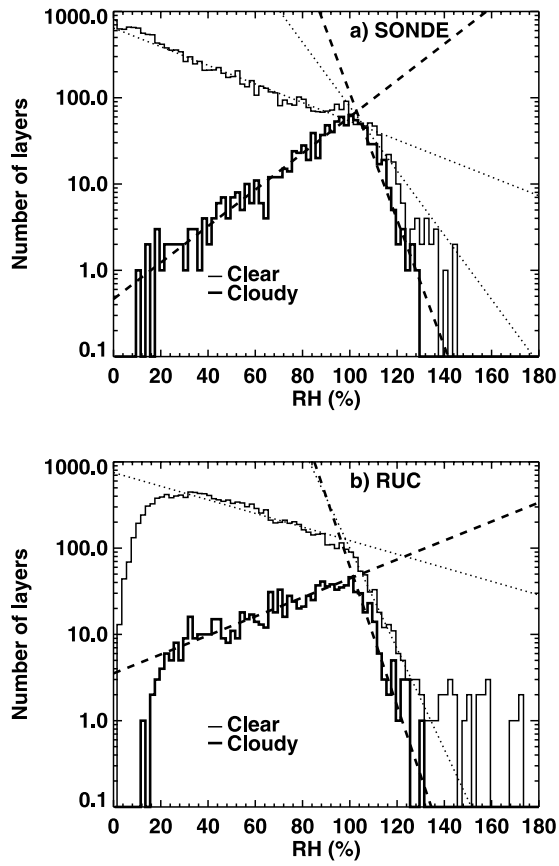

Figure 13. Frequency distributions of relative humidity in clear and cloudy, upper (100–400 hPa) tropospheric layers for (a) SONDE and (b) RUC data. Exponential fits (dotted lines) are plotted for subsaturation and supersaturation conditions.

Table 4. Slopes of Exponential Fits for SONDE and RUC

Classification		SONDE	RUC
Supersaturated region	clear layers	−0.135	−0.133
	cloudy	−0.169	−0.186
Subsaturated region	clear layers	−0.025	−0.020
	cloudy	0.049	0.025

correspond to RH values of about 90 and 80% RH for the SONDE and RUC, respectively (Figure 8). Thus, the exponential fits might be more appropriately applied using SONDE and RUC data above 90 and 80%, respectively. While it is not the same as the SONDE results, the current RUC-modeled RH follows the simple exponential distribution, indicating it provides a somewhat realistic characterization of the UTH. As noted, the adjustment for the different dry biases would probably yield similar SONDE and RUC RH distributions for the cloudy layers.

[42] The small impact of vertical motion on P_{cld} in the upper troposphere is not surprising based on previous observations. *Mace et al.* [1997] found that cirrus existed in environments in which the large-scale atmosphere was weakly ascending. Approximately 40% of cirrus occurred, however, in situations where large-scale subsidence was occurring. *Zhang* [2003] found a relatively weak dependence of high cloud amount on vertical velocity for the largest convective systems, but virtually no dependence on ω for smaller high cloud systems. Cirrus clouds are often composed of a generating cell and fall streaks that transport larger crystals into lower, dry layers where they persist for some time before finally sublimating. Thus, cirrus clouds as defined by the ARSCL will occur in both dry and moist layers. Cirrus parameterizations based on model-resolved vertical motions must account for the possibility that cirrus may form and advect through environments that are subsiding at horizontal scales comparable to the model resolution. No attempt is made here to account for any advective processes.

4.4. Previous Studies

[43] In this study, the thresholds are based on RHI for $T < 253$ K to determine how the occurrence of clouds relates to the ice saturation point. *Wang et al.* [2000] used a pair of thresholds to define a layer as being cloudy. They classified a layer as cloudy if RH > 83% at one level was adjacent to a level with RH > 87%. RHW and RHI were used for temperatures above and below 0°C, respectively. At 274 and 295 K, the 87% RH threshold would roughly correspond to P_{cld} = 40 and 70%, respectively, in Figure 8a. At temperatures below 250 K, RH = 87% is just above the P_{cld} = 40% line. These changes in probability relative to the fixed threshold indicate the need for temperature-dependent thresholds.

[44] In warmer conditions, the nonmonotonic behavior of the probability thresholds (Figure 8) likely reflects the occurrence of different processes. When $T < 273$ K, both ice and water transformation can occur so the decrease of P_{cld} with decreasing temperature below 273 K could be a result of the increasing likelihood of mixed phase processes. The decreasing values of P_{cld}, especially the smaller probabilities, with rising temperature above 275 K could be due to the more frequent occurrence of convective clouds in warmer conditions, an effect that is consistent with the greater influence of ω on the cloud probability at higher temperatures (Figure 11). This nonmonotonic behavior of P_{cld} with RH would also affect the accuracy of a constant threshold for diagnosing clouds. At 260 and 280 K, RH = 83% corresponds to P_{cld} = 60% and 40%, respectively, for the SONDE data. If the P_{cld} variability seen at the ARM SCF is typical, then past estimates of cloud layering are likely to be biased to one degree or another, depending on the layer temperature.

[45] To estimate the type of biasing that would occur, RH thresholds were computed from the results to determine the value that would result in the optimal estimate of cloud fraction over the year. The mean cloud amounts $F(T)$ for all layers within a given temperature range were computed for both data sets from the ARSCL data. The optimal humidity threshold, $RH_t(T)$, is the relative humidity threshold that satisfies

$$F(T) = N(RH > RH_t)/N_t(T), \tag{7}$$

where N_t is total number of data points for a given temperature range and $N(RH > RH_t)$ is the number of data points having $RH > RH_t$. Use of a threshold greater or less than RH_t would underestimate or overestimate, respectively, the average cloud cover in a given layer. The resulting optimal thresholds plotted in Figure 14a indicate that RH =

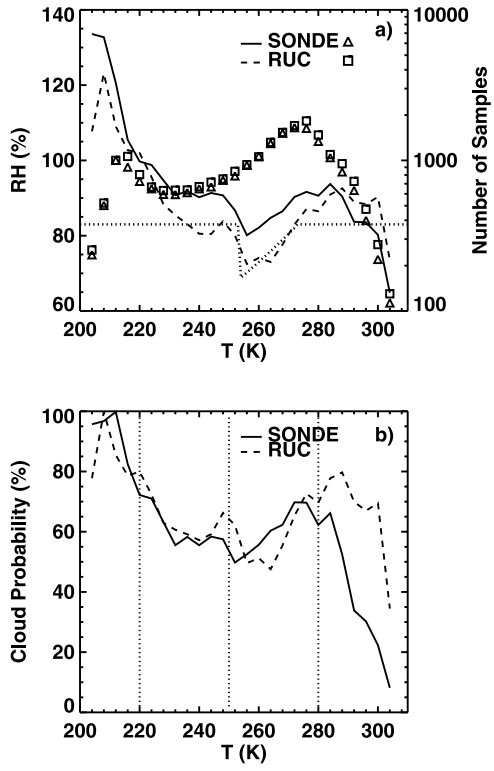

Figure 14. Optimal thresholds for obtaining the correct layer cloud amount for RUC and SONDE data. (a) RH thresholds and (b) P_{cld} thresholds. Dashed lines across Figure 14a indicate RHI = 83 and 87%. for $T < 273$ K and RHW = 83 and 87% for $T \geq 273$ K to compare the thresholds of *Wang et al.* [2000] with the optimal thresholds. Symbols denote number of samples for Figure 14a.

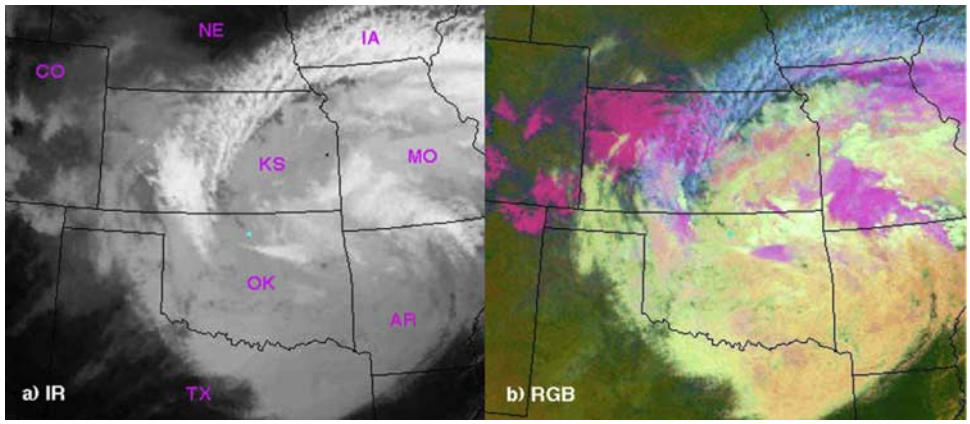

Figure 15. GOES-8 images over the ARM SGP domain at 1815 UTC, 3 March 2000, (a) infrared and (b) pseudo-color (red: 0.65-μm reflectance, green: 3.9–10.8 μm brightness temperature difference, blue: inverse 10.8-μm brightness temperature). Snow covers the surface in the bright magenta areas in CO and KS.

87% would, on average, underestimate cloud fraction at most temperatures greater than 290 K and slightly overestimate it for T between 253 and 290 K using SONDE data. The fixed threshold would also tend to overestimate cloudiness for $T < 248$ K, especially at the coldest levels. The optimal RUC RH thresholds are shifted downward. Thus, if RH = 87% were applied to detect clouds from the RUC data, it would tend to overestimate cloud amount for $T < 230$ K and underestimate cloudiness between 235 and 270 K and yield good agreement at most other temperatures. The differences between the SONDE and *Wang and Rossow* [1995] thresholds disagree with the results of *Naud et al.* [2003], who concluded that the *Wang and Rossow* [1995] thresholds need to be decreased at higher altitudes.

[46] The optimal thresholds relate to P_{cld} as shown in Figure 14b. For most temperatures, P_{cld} exceeds 50%. The exceptions occur around $T = 260$ K and for $T > 290$K. The probabilities differ from $P_{cld} = 50\%$ because all cloud amounts were used instead of just values greater than 90%. The sampling at $T > 290$ K and $T < 220$ K is significantly reduced compared to the other temperatures, so the results at these temperature extremes may not be as representative of the behavior of P_{cld} as they are for $210 \text{ K} < T < 290$ K.

[47] Although the results of this study are not directly comparable to those of *Zhang* [2003], some notable differences and similarities are evident. *Zhang* [2003] found that high cloud amount changes from 30 to 47% for RHW increasing from 15 to 80% at the 1000-km^2 scale, the one closest to that in this study. The P50 line in Figure 9a suggests that a similar behavior occurs, in relative terms, for high cloud amount. It increases from 20 to 90% for a layer RHI change of ~15%, a change slightly smaller than the *Zhang* [2003] result. The lack of a dependence of cloud amount on RUC RH for midlevel clouds in *Zhang* [2003] is not seen here. This difference might be related to the use of satellite-derived cloud heights. During the daytime, a midlevel cloud height is typically retrieved when a thin cirrus overlies a low cloud [e.g., *Minnis et al.*, 1995a] resulting in an incorrect placement of a cloud in a dry layer. At night, when only IR data are used, thin cirrus clouds are often retrieved as midlevel clouds because their semitransparency is not detectable. Such errors would tend to reduce any dependency on layer RH, because the cloud and RH are mismatched. There appears to be consistency for low clouds; the RH for a given probability increases with increasing cloud fraction (Figure 9b) while cloud amount increases with rising RH in the *Zhang* [2003] results. It is not clear if the dependencies are similar in magnitude, however, because of different formulations of the statistics. Direct comparisons would require different analyses of the current data set.

4.5. Comparison of Parameterization With Satellite-Derived Cloudiness

[48] As an initial test of the RUC-based parameterization, P_{cld} was computed for each vertical level and RUC grid box within the greater ARM SGP domain [*Minnis et al.*, 2002] at 1800 UTC, 3 March 2000. The results are compared with cloud properties derived from the Eighth Geostationary Operational Environmental Satellite (GOES) by *Minnis et al.* [2004a] using a multispectral retrieval technique [*Minnis et al.*, 1995b, 1998]. The GOES cloud products, including cloud-top and base pressures, p_{top} and p_{base}, respectively, are generated for each 4-km pixel. To compare with the RUC cloud probabilities, the GOES cloud data were used to fill a three-dimensional (3-D) RUC grid by first associating each GOES pixel with the appropriate grid box and then determining the number of pixels, N, associated with the given box. The cloud fraction within a given vertical box in the column was computed as

$$f_{pc} = N_{\Delta p}/N, \tag{8}$$

where $N_{\Delta p}$ is the number of pixels with $p_{base} \geq p_c$ and $p_{top} \leq p_c$, where p_c is the mean pressure of the RUC layer. The total cloud fraction f_t for the particular RUC grid box is the number of cloudy GOES pixels divided by N.

[49] Figure 15 shows the infrared (IR) image and a pseudo-color (RGB) image developed from GOES-8 multispectral data to highlight the different cloud types for this test case. The IR image (Figure 15a) indicates a lot of vertical structure in the scene with cirrus clouds extending

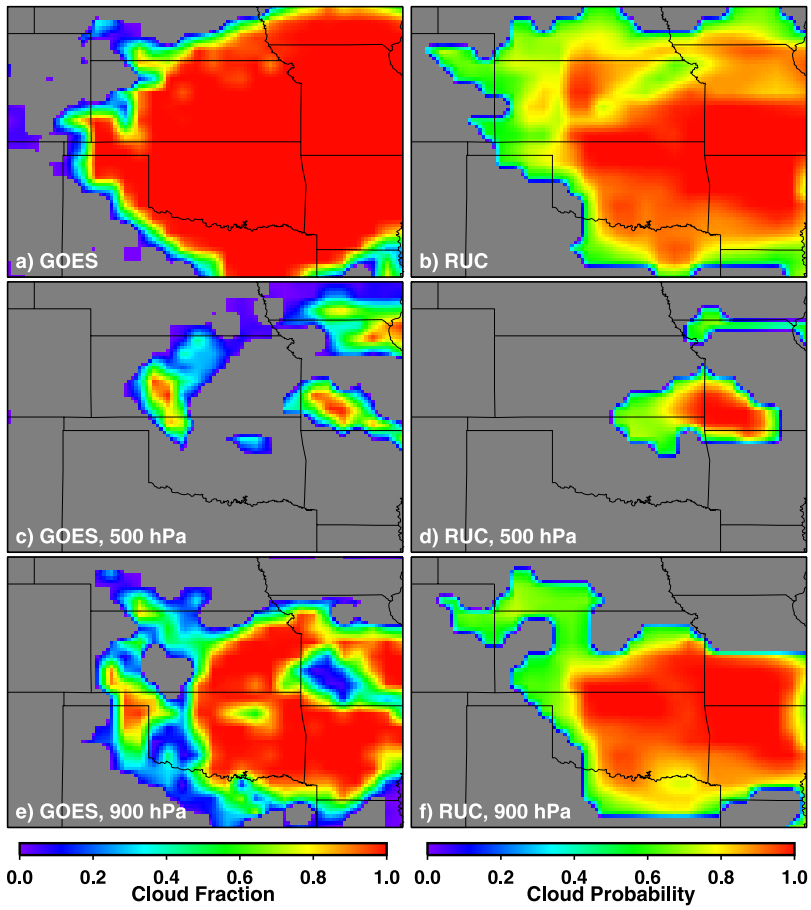

Figure 16. The 3 March 2000 cloud fractions and probabilities at two pressure levels for 1815-UTC GOES-8 and 1800-UTC RUC data over ARM SGP domain. Total coverage shown in Figures 16a and 16b.

from IA to northwestern OK over an apparent low cloud deck that appears to cover more than half the image. High and midlevel clouds also appear to cover portions of MO and northeastern OK. The true extent of cloud cover is more clearly depicted in Figure 15b. A significant portion of the apparent low cloud deck in CO and western KS actually consists of clear areas covered with snow evident as the bright magenta areas. Much of the cirrus over IA and KS has no underlying cloud deck while the remaining high and midlevel clouds appear to be above the low clouds.

[50] The horizontal distribution of cloud fractions and probabilities are shown in Figure 16 for the entire column and at two of the RUC levels, 500 and 900 hPa. Except for portions in the western half of the domain, the areas where $f_c > 10\%$ (Figure 16a) and $P_{cld} > 67\%$ (Figure 16b) are in good agreement. This probability threshold was selected because it provides the best agreement in total cloud cover. However, it puts too much cloudiness over CO and western KS and NE and too little over southwestern OK. Overall, the level of agreement is surprisingly good. Both data sets indicate significant cloudiness at 500 hPa over northern and southwestern MO and some over northeastern OK. The other area of cirrus extending from IA to northwestern OK does not appear in the RUC probabilities (Figure 16d). The satellite retrieval, however, estimates portions of it extend down to 500 hPa. The GOES cloud-top height relies on the accuracy of the visible optical depth retrieval which is not very good for thin clouds over snow surfaces like those over central and western KS. Given the IR image, it is unclear whether the GOES retrieval overestimates f_{500} in the western area, but it is too large in central KS. The retrieved cloud-top heights vary between 9 and 11 km for much of the cirrus except over central KS where it drops to between 4 and 6 km, most likely because the snow causes an overestimation of cloud optical depth. At 900 hPa, the GOES (Figure 16e) and RUC (Figure 16f) agree well over AR and eastern OK and KS but not very well over TX, CO, and western MO. The GOES retrievals place much of the cloud cover over northern TX and western KS at a slightly lower pressure than 900 hPa. Part of the area with $P_{cld} > 67\%$ has no cloud cover as discussed earlier. One of the interesting features in this comparison is the hole in f_{900} over southwestern MO, where $P_{cld} > 90\%$. Given that the higher clouds observed by the satellite block the view to the lower cloud and the low cloud cover is continuous around the hole, it is likely that RUC provides a more accurate depiction of cloudiness at this pressure level.

[51] Three-dimensional views of the resulting cloud fields are shown in Figure 17 for $f_t > 10\%$ and for $P_{cld} > 67\%$. In addition to the differences seen in Figure 16, the 3-D images show that the RUC (Figure 17b) produces continuous cirrus layers around 200 hPa in two branches

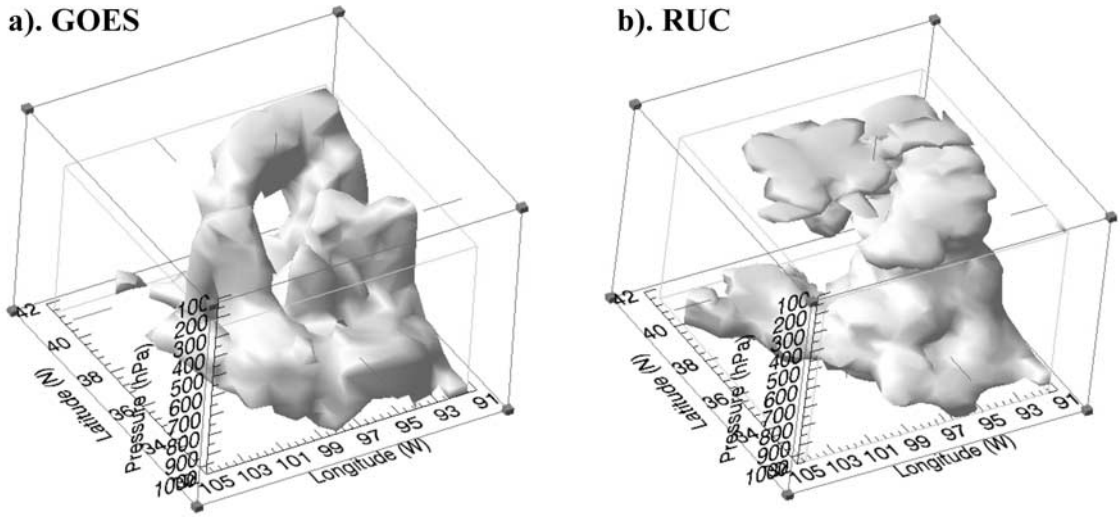

Figure 17. Three-dimensional plot of 3 March 2000 cloud volumes over ARM SGP domain at (a) 1815 UTC from GOES-8 for cloud amounts greater than 10% and (b) 1800 UTC from RUC for cloud probabilities greater than 67%.

that extend southwestward and westward from the northeastern corner of the domain. The GOES retrieval (Figure 17a) shows decks in the same areas, but they are much less continuous than their RUC counterparts. The GOES-retrieved southwestern branch is broken up into three main portions as seen in Figure 16c and is more consistent with the imagery. Conversely, the RUC produces a more realistic depiction of the northern cirrus cloud deck over KS. It is more in accord with the IR image than the GOES retrieval. However, it inserts a deck of low clouds in that same area where few are evident. In this situation, the high cloud blocks the GOES view of the low cloud deck.

[52] Although this preliminary example is not conclusive, it suggests that the RUC RH field can be used to produce a realistic depiction of the vertical structures of clouds and demonstrates the potential utility of this type of analysis. With the proper logic, P_{cld} could be used together with the GOES results to fill in the clouds at lower levels when they are obscured by higher level clouds. Conversely, the RUC would be ignored for areas where the RUC RH indicates cloudiness but the satellite analysis finds none. Development of the complex logic needed to reliably combine the RUC and satellite data is left for future research.

5. Concluding Remarks

[53] This paper has provided a quantitative comparison between relative humidities and cloud cover for two different meteorological data sets over the ARM SCF. Both types of data can be used to estimate the occurrence of cloud cover in the vertical although the radiosonde data are probably more reliable than the RUC data, as expected. The probabilities for finding a cloud layer at a particular relative humidity are temperature dependent and are slightly enhanced by upward vertical motion especially in the lower troposphere. At a given relative humidity and temperature, the RUC probabilities for cloud occurrence are generally greater than those for the radiosonde. This difference is primarily due to a greater number of mismatches between the actual cloud height and the moist layer and probably, to a lesser extent, due to a greater dry bias at colder temperatures as a result of the model to assimilation of operational radiosondes. The RUC relative humidities are comparable for clear layers in the middle and lower troposphere, but the RUC is ~10% drier, on average, at all levels in cloudy conditions. This suggests that the RUC is drying the atmosphere too much in cloudy conditions, perhaps as a result of cloud formation within the model. This aspect warrants further investigation as it could impact the formulation of the RUC cloud parameterizations. Overall, the RUC relative humidity analysis can be used as if it were a radiosonde data set as a means to determining the locations of clouds. As reflected in the probability thresholds, however, the RUC and SONDE data cannot be used interchangeably.

[54] The RUC20 model with 20-km horizontal resolution replaced the RUC-2 model during April 2002 and other changes are continuing [*Benjamin et al.*, 2004c]. To improve quantitative precipitation forecasts, several changes in the way the model handles UTH were made. The tropopause is more sharply defined, and most ice supersaturations for pressure levels less than 300 hPa are removed [*Benjamin et al.*, 2004a]. These changes dry the upper troposphere relative to that in the RUC-2. Thus, the relative humidity thresholds used to make the cloud diagnoses for the RUC20 data need to be reinvestigated and determined for RUC20, especially for the upper troposphere. Additional changes could require more tuning of the thresholds.

[55] The thresholds and cloud probability models developed here are based on data taken over a 1-year period at one location. The probabilities for estimating cloud occurrence at other locations or using other numerical weather prediction/assimilation models or radiosonde types could be different than those developed here. Additional study would be required to determine the accuracy of using the simple thresholds developed here in those other conditions. The models could be tested using ARSCL-like products from

other ARM locations and similarly equipped sites. Future research that could be useful for defining cloud properties from both radiosonde and model data should focus on the relationships between cloud type and water content and the humidity, temperature, and vertical velocity fields as well as the seasonal and diurnal aspects of the RH thresholds. Similar analyses using both the ARSCL and GOES cloud data sets could be used to validate the cloud condensate generated by the RUC.

[56] The results of this study should be valuable for improving cloud parameterizations and for development of improved methods for validating model-generated cloud properties. Additionally, the results could be used together with the satellite data to better determine the three-dimensional structure of a cloud field. Such fields would be valuable for initializing and validating larger-scale models and for computing the radiative heating rates at all levels of the atmosphere. If combined in a near-real time fashion, the resultant data set could be used to more reliably diagnose aircraft icing conditions even when high clouds obscure the low-level ''offending'' cloud. To occur in a timely fashion, short-term RUC forecasts would be used instead of analyses. Thus, the type of study performed here should be repeated using RUC forecasts at different times relative to the initialization of the forecast.

[57] **Acknowledgments.** This research was supported by the Office of Biological and Environmental Research of U.S. Department of Energy through the Interagency Agreements DE-AI02-97ER62341 and DE-AI02-02ER63319 as part of the Atmospheric Radiation Measurement Program. Support was also provided by the NASA Aviation Safety Program through the NASA Advanced Satellite Aviation-Weather Products Initiative. The authors are grateful to D. R. Doelling, M. M. Khaiyer, and M. L. Nordeen for valuable discussions and ARSCL data preparation and to an anonymous reviewer who made many good suggestions and provided some valuable information.

References

Ackerman, T., and G. Stokes (2003), The Atmospheric Radiation Measurement Program, *Phys. Today*, *56*, 38–45.

Baum, B. A., R. F. Arduini, B. A. Wielicki, P. Minnis, and S.-C. Tsay (1994), Multilevel cloud retrieval using multispectral HIRS and AVHRR data: Nighttime oceanic analysis, *J. Geophys. Res.*, *99*, 5499–5514.

Benjamin, S. G., J. M. Brown, K. J. Brundage, B. E. Schwartz, T. G. Smirnova, and T. L. Smith (1998), The operational RUC-2, in *Proceedings of 16th Conference on Weather Analysis and Forecasting, Phoenix, AZ, January 11–16*, pp. 249–252, Am. Meteorol. Soc., Boston, Mass.

Benjamin, S. G., G. A. Grell, J. M. Brown, T. G. Smirnova, and R. Bleck (2004a), Mesoscale weather prediction with the RUC hybrid isentropic/terrain-following coordinate model, *Mon. Weather Rev.*, *132*, 474–494.

Benjamin, S. G., et al. (2004b), An hourly assimilation/forecast cycle: The RUC, *Mon. Weather Rev.*, *132*, 495–518.

Benjamin, S. G., T. G. Smirnova, K. Brundage, S. S. Weygandt, T. L. Smith, B. Schwartz, D. Dévényi, J. M. Brown, and G. A. Grell (2004c), A 13-km RUC and beyond: Recent developments and future plans, in *Proceedings of 11th Conference on Aviation, Range, and Aerospace, Hyannis, MA, October 4–8* [CD-ROM, J1.6], Am. Meteorol. Soc., Boston, Mass.

Chernykh, I. V., and R. E. Eskridge (1996), Determination of cloud amount and level from radiosonde soundings, *J. Appl. Meteorol.*, *35*, 1362–1369.

Clothiaux, E. E., R. C. Perez, D. D. Turner, T. P. Ackerman, G. G. Mace, K. P. Moran, R. T. Marchand, M. A. Miller, and B. E. Martner (2000), Objective determination of cloud heights and radar reflectivities using a combination of active remote sensors at the ARM CART sites, *J. Appl. Meteorol.*, *39*, 645–665.

Clothiaux, E. E., et al. (2001), The ARM Millimeter Wave Cloud Radars (MMCRs) and the Active Remote Sensing of Clouds (ARSCL) Value Added Product (VAP), *DOE Tech. Memo. ARM VAP-002.1*, 56 pp., Dep. of Energy, Washington, D. C. (Available at http://www.arm.gov/publications/tech_reports/armvap-002-1.pdf)

Duda, D. P., P. Minnis, L. Nguyen, and R. Palikonda (2004), A case study of the development of contrail clusters over the Great Lakes, *J. Atmos. Sci.*, *61*, 1132–1146.

Ghan, S., et al. (2000), A comparison of single column model simulations of summertime midlatitude continental convection, *J. Geophys. Res.*, *105*, 2091–2124.

Gierens, K. (1996), Numerical simulations of persistent contrails, *J. Atmos. Sci.*, *53*, 3333–3348.

Gierens, K., U. Schumann, M. Helten, H. G. J. Smit, and A. Marenco (1999), A distribution law for relative humidity in the upper troposphere and lower stratosphere derived from three years of MOZAIC measurements, *Ann. Geophys.*, *17*, 1218–1226.

Huang, J., P. Minnis, B. Lin, Y. Yi, M. M. Khaiyer, R. F. Arduini, and G. G. Mace (2005), Advanced retrievals of multilayered cloud properties using multisensor and multispectral measurements, *J. Geophys. Res.*, *110*, D15S18, doi:10.1029/2004JD005101.

Kawamoto, K., P. Minnis, W. L. Smith Jr., and A. D. Rapp (2002), Detecting multilayer clouds using satellite solar and IR channels, in *Proceedings of 11th Conference on Cloud Physics., Ogden, UT, June 3–7* [CD-ROM, JP1.18], Am. Meteorol. Soc., Boston, Mass.

Lin, B., P. Minnis, B. A. Wielicki, D. R. Doelling, R. Palikonda, D. F. Young, and T. Uttal (1998), Estimation of water cloud properties from satellite microwave and optical measurements in oceanic environments: 2. Results, *J. Geophys. Res.*, *103*, 3887–3905.

Lindzen, R. S. (1990), Some coolness concerning global warming, *Bull. Am. Meteorol. Soc.*, *71*, 288–299.

Mace, G., T. Ackerman, E. Clothiaux, and B. Albrecht (1997), A study of composite cirrus morphology using data from a 94-GHz radar and correlations with temperature and large-scale vertical motion, *J. Geophys. Res.*, *102*, 13,581–13,594.

Mace, G., T. P. Ackerman, P. Minnis, and D. F. Young (1998a), Cirrus layer microphysical properties derived from surface-based millimeter radar and infrared interferometer data, *J. Geophys. Res.*, *103*, 23,207–23,216.

Mace, G., C. Jakob, and K. Moran (1998b), Validation of hydrometeor occurrence predicted by the ECMWF model using millimeter wave radar data, *Geophys. Res. Lett.*, *25*, 1645–1648.

Miloshevich, L. M., H. Vömel, A. Paukkunen, A. J. Heymsfield, and S. J. Oltmans (2001), Characterization and correction of relative humidity measurements from Vaisala RS80-A radiosondes at cold temperatures, *J. Atmos. Oceanic Technol.*, *18*, 135–156.

Miloshevich, L. M., A. Paukkunen, H. Vömel, and S. J. Oltmans (2004), Development and validation of a time-lag correction for Vaisal radiosonde humidity measurements, *J. Atmos. Oceanic Technol.*, *21*, 1305–1327.

Minnis, P., W. L. Smith Jr., D. P. Garber, J. K. Ayers, and D. R. Doelling (1995a), Cloud properties derived from GOES-7 for the spring 1994 ARM intensive observing period using version 1.0.0 of the ARM satellite data analysis program, *NASA RP, 1366*, 59 pp.

Minnis, P., D. P. Kratz, J. A. Coakley Jr., M. D. King, D. Garber, P. Heck, S. Mayor, D. F. Young, and R. Arduini (1995b), Cloud optical property retrieval (subsystem 4.3), in *Clouds and the Earth's Radiant Energy System (CERES) Algorithm Theoretical Basis Document*, vol. 3, *Cloud Analyses and Radiance Inversions (Subsystem 4)*, edited by CERES Science Team, *NASA RP, 1376*, 135–176.

Minnis, P., D. P. Garber, D. F. Young, R. F. Arduini, and Y. Takano (1998), Parameterization of reflectance and effective emittance for satellite remote sensing of cloud properties, *J. Atmos. Sci.*, *55*, 3313–3339.

Minnis, P., W. L. Smith Jr., D. F. Young, L. Nguyen, A. D. Rapp, P. W. Heck, and M. M. Khaiyer (2002), Near-real-time retrieval of cloud properties over the ARM CART area from GOES data, in *Proceedings of 12th Science Team Meeting, April 8–12, St. Petersburg, FL*, 7 pp., Atmos. Radiat. Meas. Program, Washington, D. C. (Available at http://www.arm.gov/docs/documents/technical/conf_0204/minnis-p.pdf)

Minnis, P., J. K. Ayers, M. L. Nordeen, and S. P. Weaver (2003), Contrail frequency over the United States from surface observations, *J. Clim.*, *16*, 3447–3462.

Minnis, P., et al. (2004a), Real-time cloud, radiation, and aircraft icing parameters from GOES over the USA, in *Proceedings of 13th Conference on Satellite Oceanography and Meteorology, Norfolk, VA, Sept. 20–24* [CD-ROM, P7.1], Am. Meteorol. Soc., Boston, Mass.

Minnis, P., J. K. Ayers, R. Palikonda, and D. N. Phan (2004b), Contrails, cirrus trends, and climate, *J. Clim.*, *17*, 1671–1685.

Naud, C. M., J.-P. Muller, and E. E. Clothiaux (2003), Comparison between active sensor and radiosonde cloud boundaries over the ARM Southern Great Plains site, *J. Geophys. Res.*, *108*(D4), 4140, doi:10.1029/2002JD002887.

Nordeen, M. L., P. Minnis, M. M. Khaiyer, D. R. Doelling, and D. Phan (2005), Comparison of surface and satellite-derived cloud and radiation properties at the ARM SGP and TWP sites, in *Proceedings of 15th Science Team Meeting, Daytona Beach, FL, March 14–18*,

Atmos. Radiat. Meas. Program, Washington, D. C. (Available at http://www.arm.gov/publications/proceedings/conf15/extended_abs/nordeen_ml.pdf)

Ovarlez, J., J.-F. Gayet, K. Gierens, J. Strom, H. Ovarlez, F. Auriol, R. Busen, and U. Schumann (2002), Water vapor measurements inside cirrus clouds in northern and southern hemispheres during INCA, *Geophys. Res. Lett.*, *29*(16), 1813, doi:10.1029/2001GL014440.

Pavlonis, M. J., and A. K. Heidinger (2004), Daytime cloud overlap detection from AVHRR and VIIRS, *J. Appl. Meteorol.*, *43*, 762–778.

Pierrehumbert, R. T. (1994), Thermostats, radiator fins and local runaway greenhouse, *J. Atmos. Sci.*, *52*, 1784–1806.

Poore, K. D., J. Wang, and W. B. Rossow (1995), Cloud layer thicknesses from a combination of surface and upper-air observations, *J. Clim.*, *8*, 550–568.

Rind, D., E. W. Chiou, W. Chu, J. Larsen, S. Oltmans, J. Lerner, M. P. McCormick, and L. McMaster (1991), Positive water vapour feedback in climate models confirmed by satellite data, *Nature*, *349*, 500–503.

Sassen, K. (1997), Contrail-cirrus and their potential for regional climate change, *Bull. Am. Meteorol. Soc.*, *78*, 1885–1903.

Spichtinger, P., K. Gierens, and W. Read (2002), The statistical distribution law of relative humidity in the global tropopause region, *Meteorol. Z.*, *11*, 83–88.

Spichtinger, P., K. Gierens, U. Leiterer, and H. Dier (2003), Ice supersaturation in the tropopause region over Lindenberg, Germany, *Meteorol. Z.*, *12*, 143–156.

Turner, D., B. Lesht, A. Clough, J. Liljegren, H. Revercomb, and D. Tobin (2003), Dry bias and variability in Vaisala RS80-H radiosondes: The ARM experience, *J. Atmos. Oceanic Technol.*, *20*, 117–132.

Wang, J., and W. B. Rossow (1995), Determination of cloud vertical structure from upper-air observations, *J. Appl. Meteorol.*, *34*, 2243–2258.

Wang, J., W. B. Rossow, and Y. Zhang (2000), Cloud vertical structure and its variations from a 20-yr global rawinsonde data set, *J. Clim.*, *13*, 3041–3056.

Wang, J., H. Cole, D. J. Carlson, E. R. Miller, K. Beierle, A. Paukkunen, and T. K. Laine (2002), Corrections of humidity measurement errors from the Vaisala RS80 radiosonde: Application to TOGA/COARE data, *J. Atmos. Oceanic Technol.*, *19*, 981–1002.

Wang, J., D. J. Carlson, D. B. Parsons, T. F. Hock, D. Lauritsen, H. L. Cole, K. Beierle, and E. Chamberlain (2003), Performance of operational radiosonde humidity sensors in direct comparison with a chilled mirror dew-point hygrometer and its climate implication, *Geophys. Res. Lett.*, *30*(16), 1860, doi:10.1029/2003GL016985.

Zhang, G. (2003), Lagrangian study of cloud properties and their relationships to meteorological parameters over the U.S. Southern Great Plains, *J. Clim.*, *16*, 2700–2716.

K. Ayers, J. Huang, P. Minnis, and Y. Yi, NASA Langley Research Center, Hampton, VA 23681, USA. (p.minnis@larc.nasa.gov)